THE ASTROPHYSICAL JOURNAL, 479:82–89, 1997 April 10

THE REAL SPACE AND REDSHIFT SPACE CORRELATION FUNCTIONS AT REDSHIFT $z = 1/3$

C. W. SHEPHERD,[1] R. G. CARLBERG,[1,2] H. K. C. YEE,[1,2] AND E. ELLINGSON[2,3]
Received 1996 January 3; accepted 1996 November 4

ABSTRACT

We present the results of a study of the two-point correlation function for a sample of field galaxies taken from the Canadian Network for Observational Cosmology cluster survey. The sample consists of 183 galaxies within a contiguous region of sky covering 216 square arcminutes. The objects have r-band magnitudes $17.0 \leq r \leq 21.7$ and redshifts $0.21 \leq z \leq 0.53$. The median redshift of the sample is 0.37. We fit the real space correlation function to a power law $\xi(r) = (r/r_0)^{-1.7}$, finding $r_0 = 1.9^{+0.4}_{-0.4}\ h^{-1}$ Mpc ($\Omega_0 = 1$), or $r_0 = 2.2^{+0.5}_{-0.4}\ h^{-1}$ Mpc ($\Omega_0 = 0.2$); uncertainties are estimated using the bias-corrected bootstrap resampling method, with 300 resamplings. This low correlation length implies strong evolution has occurred in the correlation function; if the observed correlation function is modeled as $\xi(r, z) = \xi(r, 0)(1 + z)^{-(3+\varepsilon)}$ with $\xi(r, 0) = (r/5.1\ h^{-1}\ \mathrm{Mpc})^{-1.7}$, then $\varepsilon \approx 1.5$. Comparison of the redshift space and real space correlation functions indicates that the one-dimensional pairwise peculiar velocity dispersion σ at $z \approx 0.37$ is weakly inconsistent with 720 km s^{-1}, the value predicted by the cosmic virial theorem if $\Omega_0 = 1$. The observed correlation functions are, however, consistent with $\sigma \approx 360$ km s^{-1}, the value expected if $\Omega_0 = 0.2$.

Subject headings: galaxies: clusters: general — galaxies: distances and redshifts — galaxies: evolution

1. INTRODUCTION

The study of galaxy clustering has yielded important information about the large-scale structure of the universe and about the environment of galaxies. One of the most useful statistics employed in this study is the two-point correlation function. This statistic quantifies the clustering of galaxies and is directly related to the power spectrum of density fluctuations in the galaxy distribution. The correlation function, when estimated from data from redshift surveys, also yields information about the dynamics of clustering. Determining the evolution of the correlation function is therefore essential for an understanding of cosmological structure formation.

The two-point correlation function has been extensively studied at low redshifts; Efstathiou (1995) gives a summary of redshift surveys that have been used for correlation analysis. Observations of the correlation function at the present epoch indicate that it is well described by a power law,

$$\xi(r) = \left(\frac{r}{r_0}\right)^{-\gamma}, \tag{1}$$

at scales $r \lesssim 10\ h^{-1}$ Mpc. Here, and throughout this paper, all separations are given in physical, as opposed to comoving, coordinates unless otherwise stated; the Hubble parameter is taken to be $H_0 = 100\ h$ km s^{-1} Mpc^{-1}. Results from optical surveys of nearby galaxies include $r_0 = 5.4 \pm 0.3\ h^{-1}$ Mpc, $\gamma = 1.77 \pm 0.04$ from the Center for Astrophysics (CfA) survey (Davis & Peebles 1983), $r_0 = 5.1 \pm 0.2\ h^{-1}$ Mpc, $\gamma = 1.71 \pm 0.05$ from the Stromlo-APM survey (Loveday et al. 1995), and $r_0 = 5.0 \pm 0.1\ h^{-1}$ Mpc, $\gamma = 1.79 \pm 0.04$ from the Las Campanas Redshift survey (Lin 1995). For the purposes of comparing our results to those from local samples, we adopt $r_0 = 5.1\ h^{-1}$ Mpc and $\gamma = 1.7$.

The principal aim of this investigation is to examine the evolution of the correlation function. A useful empirical model for this evolution, introduced by Koo & Szalay (1984) is

$$\xi(r, z) = \xi(r, 0)(1 + z)^{-(3+\varepsilon)}. \tag{2}$$

In this model, $\varepsilon = \gamma - 3$ corresponds to clustering fixed in comoving coordinates, as seen in biased cold dark matter (CDM) simulations (Carlberg 1991). If $\varepsilon = 0$, clustering is stable in physical coordinates. Colin, Carlberg, & Couchman (1996) find $\varepsilon \sim 0$ for an open CDM (OCDM) initial power spectrum with $\Omega_0 = 0.2$.

To determine ε, one must compute the correlation function for objects at an earlier epoch. In the absence of redshift data, an estimate of the spatial correlation function may be obtained by computing the angular correlation function (e.g., Koo & Szalay 1984; Efstathiou et al. 1991; Infante & Pritchet 1995). This method does not require that the distances to the objects in the sample be known; rather, the clustering is observed as a two-dimensional projection of the three-dimensional clustering over a wide range of redshifts. In order to estimate the amount of clustering evolution present in the data, therefore, models for both the correlation function and its evolution and the redshift distribution of objects in the sample must be assumed; r_0 is not directly determined at any particular epoch. Using this method, Efstathiou et al. (1991) and Infante & Pritchet (1995) find $\varepsilon > 0$ if $\Omega_0 = 1$, under the assumption that there is no evolution in the luminosity function.

In order to produce a reliable estimate of the spatial two-point correlation function from redshift data, redshifts for a large number of objects must be obtained. Pencil-

[1] Department of Astronomy, University of Toronto, Toronto, ON, Canada M5S 3H8.
[2] Guest observer, Canada-France-Hawaii Telescope, operated jointly by National Research Council of Canada Centre Nationale de la Recherche Scientifique of France, and the University of Hawaii.
[3] Center for Astrophysics and Space Astronomy, University of Colorado, Campus Box 389, Boulder, CO 80309-0389.

beam surveys using multiobject spectroscopy (MOS), such as the Autofib survey (Cole et al. 1994) and the Canada-France Redshift Survey (CFRS; Le Fèvre et al. 1996) are the only surveys to date which contain a sufficient number of objects at intermediate redshifts. Le Fèvre et al. (1996) find $\varepsilon \sim 0$–2 in the CFRS survey, consistent with the evolution observed in angular surveys.

In principle, data from pencil-beam surveys may be used to estimate the redshift space correlation function. The required velocity accuracy is, however, quite high. Davis & Peebles (1983) find the one-dimensional pairwise peculiar velocity dispersion in the CfA survey to be $\sigma = 340 \pm 40$ km s^{-1} at a separation of 1 h^{-1} Mpc. If the velocity errors in a survey are comparable to $\sigma/2^{1/2}$, computation of a reliable redshift space correlation function from that survey is impossible. Cole et al. (1994) find a comoving correlation length $r_0 = 6.5 \pm 0.4\ h^{-1}$ Mpc based on the redshift space correlation function for the Autofib survey. The median redshift of this survey is $\bar{z} = 0.16$; taking $r_0(z = 0.16) = 6.5/1.16\ h^{-1}$ Mpc and $r_0(z = 0) = 5.1\ h^{-1}$ Mpc in equation (2) yields $\varepsilon \approx -4$, at odds with previous angular correlation results.

We present here estimates of the real space and redshift space two-point correlation function for a sample of field galaxies taken from the Canadian Network for Observational Cosmology (CNOC) cluster survey. The data are described in § 2. The techniques used for computing the real space two-point correlation function and its evolution, along with the results for this survey, are presented in § 3. Also described there is our investigation of the redshift space two-point correlation function and the heretofore unknown pairwise peculiar velocity dispersion at $z \sim 0.37$. Our conclusions are given in § 4.

2. DATA

The data used here are taken from the CNOC cluster survey. The observational procedures and data reduction are described in detail in Yee, Ellingson, & Carlberg (1996). The data were obtained using the multiobject spectrograph (MOS) at the Canada-France-Hawaii Telescope (CFHT). A band-limiting filter was used with the spectrograph to reduce the wavelength range of each spectrum, further increasing the multiplexing rate. One patch in the survey, MS1512+36, is well suited to a correlation analysis of field galaxies since the cluster is quite poor. Only data from this field are analyzed here; the complete catalog is presented in Abraham et al. (1997).

Pencil-beam surveys present several problems related to the fairness of the sample (a sample is fair if the structure contained within it is representative of the global average). The first difficulty relates to the beam width; if the beam diameter is similar to r_0, then the distribution of objects in a beam may be dominated by a single large density inhomogeneity, biasing the estimation of ξ. One possible solution to this problem is to calculate the correlation function from data taken from many narrow pencil-beams scattered randomly throughout the sky. However, this approach does not make optimal use of the data; it is preferable to place the beams so that the beam-beam separation is comparable to the beamwidth, thus increasing the number of pairs of objects with separations on the order of r_0. The MS1512+36 data are from a mosaic of three fields from the survey, with a total angular size of $27' \times 8'$ (216 square arcmin). The width of the sample at $z = 0.37$ is $\sim 6.8\ h^{-1}$ Mpc ($\Omega_0 = 1$), sufficiently large for an investigation of clustering on scales $\sim r_0$.

A second complication with MOS data is that of selection effects. Magnitude selection may bias the sample toward bright objects, which will lead to erroneous results if bright objects cluster differently from faint objects. More importantly, MOS produces a lower limit on the separation of objects for which spectra may be observed. Once one object is designated to be observed through a slit on a given mask, the placement of the spectra on the detector precludes designing another slit closely above or below the first. This can result in high density regions being sampled less completely than low density regions, possibly reducing the observed correlation. Each of the three fields composing the MS1512+36 data was observed with 2 different MOS masks, with a higher priority given in the second mask to completing observations of closely spaced pairs (see Yee et al. 1996 for details). This use of multiple masks somewhat reduces the amount of geometric selection; the remaining selection is corrected by weighting the data as described below.

To correct for the magnitude and geometric selection, a magnitude weight w_m and local magnitude weight $w_{\rm lm}$ are calculated from the data for each object in the sample. For a given object with apparent magnitude in the bin $(m, m + \Delta m)$ and observed redshift z, w_m is proportional to the fraction of objects anywhere in the sample in the same magnitude bin which have observed redshifts. The local magnitude weight $w_{\rm lm}$ for an object is proportional to the fraction of objects in a circle with radius $2'$ about the first object in the same magnitude bin which have observed redshifts. Also defined for each object is the geometric weight $w_{xy} = w_{\rm lm}/w_m$, which is related to the number of nearby objects at any magnitude which have observed redshifts. A detailed explanation of the weighting procedure is given in Yee et al. (1996). A test of the extent to which these weights correct for the sampling nonuniformities is described in § 3.1; it is found that the weighting procedure adequately offsets the selection effects.

Four subsamples of the MS1512+36 catalog are created: the photometric, redshift, field, and extended field samples. The photometric sample, used for computing the angular correlation function, consists of the 404 objects with photometry in both the Gunn g- and r-bands, with r-band magnitude in the range $17.0 \leq r \leq 21.7$. The upper magnitude limit is chosen so that the magnitude weight of every object in the redshift sample is less than 5; the lower limit is employed since the masks were designed to exclude objects much brighter than the brightest cluster galaxy, which has $r = 18.45$.

The redshift sample consists of the 183 objects in the photometric sample which have identified redshifts in the range $0.21 \leq z \leq 0.53$; the median redshift of this sample is 0.37. These limits are chosen so that the spectral features used to identify emission line objects lie within the optimal response region of the filter. This sample is shown in Figure 1. In this analysis we have extended the lower z limit from 0.27 in Yee et al. (1996) to 0.21. The original higher limit was based on the detection of [O II] λ3727 at the blue end of the spectrum. However, the wavelength limits for the filter used are such that as [O II] λ3727 disappears at the blue end, the [O III] $\lambda\lambda$4959, 5007 lines come in on the red end. From our sample, we have found that whenever the [O III] $\lambda\lambda$4959, 5007 and [O II] λ3727 lines are both within the spectral

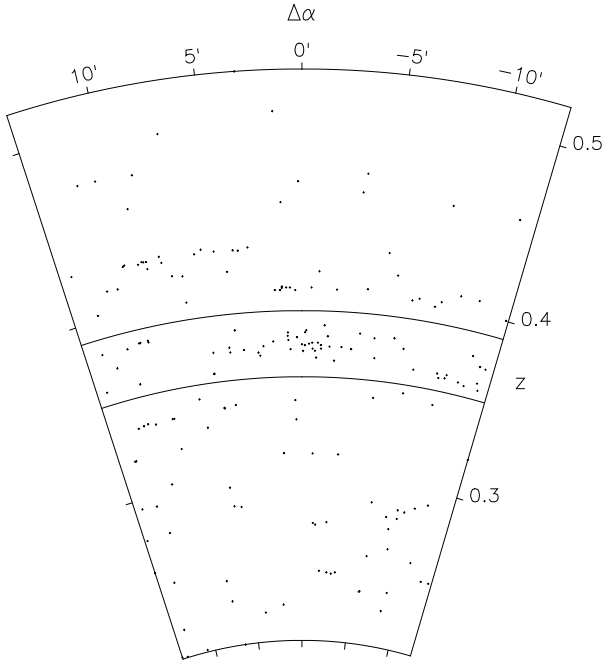

FIG. 1.— MS 1512+36 redshift sample. The angular scale has been expanded by a factor of ~80. The objects within the central box are taken to be potential cluster members; they not included in the field sample and are weighted less than the field objects in the extended field sample, as described in the text.

range, they are always detected simultaneously. Hence we can safely use the [O III] λλ4959, 5007 lines to extend our lower redshift limit; no significant selection bias as a function of spectral type is seen in the redshift sample (Yee et al. 1996).

The field sample is constructed from the redshift sample by removing the 61 objects that have redshifts $0.354 \leq z \leq 0.390$. These redshift limits correspond to the limits of the cluster (from Carlberg et al. 1996) enlarged by $z = 0.01$ in both directions; the field sample therefore almost certainly excludes all cluster members. The field sample contains 122 objects, with a median redshift of 0.34.

The extended field sample is the same as the redshift sample, except that the 61 objects within the enlarged cluster redshift limits $0.354 \leq z \leq 0.390$ have their local magnitude weights reduced by a factor of 0.25. This reduction factor is the ratio of the comoving number density of objects in the field sample to the density within the enlarged cluster redshift limits. This construction therefore removes the bias toward high density regions present in the redshift sample, while making full use of all the redshift data available.

3. ANALYSIS

3.1. *Estimating the Correlation Function*

The two-point correlation function ξ is defined by (Peebles 1980)

$$\delta P(r) = \bar{n}[1 + \xi(r)]\delta V \,, \tag{3}$$

where $\delta P(r)$ is the probability of finding a second object in a volume δV with a physical separation r from a randomly chosen object and $\bar{n}$ is the mean density of objects. For a finite sample of objects and some (small) fixed separation difference Δr, $\xi(r)$ may be estimated from equation (3) as

$$1 + \xi(r) \approx \frac{\mathrm{DD}(r)}{N_D^2} \frac{V}{\Delta V(r)} \,. \tag{4}$$

Here, N_D is the number of objects in the sample, DD(r) is the number of ordered pairs of objects in the sample with separation between r and $r + \Delta r$, V is the volume of the sample, and $\Delta V(r)$ is the average volume of the set surrounding a first object in which a second may be found with separation between r and $r + \Delta r$ from the first.

The volumes ΔV in equation (4) are estimated using Monte Carlo integration. A random data set containing N_R objects is generated within the volume of the original data set in a manner such that the random catalog is subject to the same selection criteria as the data. If the number of pairs of objects with separation between r and $r + \Delta r$, the first object belonging to the data set, the second to the random set, is DR(r), then

$$1 + \xi(r) \approx \frac{N_R}{N_D} \frac{\mathrm{DD}(r)}{\mathrm{DR}(r)} \tag{5}$$

(Davis & Peebles 1983).

The pair counts DD and DR in equation (5) may be computed with arbitrary weights, so that $\mathrm{DD}(r) = \sum_{i,j} w_i^{(D)} w_j^{(D)}$ and $\mathrm{DR}(r) = \sum_{i,j} w_i^{(D)} w_j^{(R)}$, where the sums are taken over all data-data or data-random pairs of objects with separation between r and $r + \Delta r$, respectively, and $w_i^{(D)}$ and $w_i^{(R)}$ are the weights to be applied to ith data and random object, respectively. The object counts N_D and N_R in equation (5) are replaced with the weighted object counts $D = \sum_{i=1}^{N_D} w_i^{(D)}$ and $R = \sum_{i=1}^{N_R} w_i^{(R)}$, respectively. The correlation function is then estimated as

$$1 + \xi(r) \approx \frac{R}{D} \frac{\mathrm{DD}(r)}{\mathrm{DR}(r)} \,. \tag{6}$$

To correct for the selection effects present in this sample, the weights used for computing the pair and object counts defined above are the local magnitude weights w_{lm}.

The selected random catalog is generated by first creating a uniform random catalog, by randomly distributing objects throughout the sample volume in such a way that the comoving density of objects is constant. Apparent magnitudes are then assigned to each object in the uniform random catalog using the process described below, and those objects lying outside the magnitude limits of the survey are discarded. Finally, the local magnitude selection is estimated at the angular position of each object-random object, and objects failing the selection criteria are discarded. For small data sets, this method is preferable to smoothing the observed redshift distribution, since the redshift distribution is dominated by density inhomogeneities comparable to the width of the sample, making the random distribution obtained sensitive to the smoothing window used.

Absolute magnitudes for the objects in the field sample are required to determine the luminosity function, which is used for generating the absolute magnitudes for the random objects. The K-corrections are obtained by interpolating from model K-corrections in the r and g bands as a function of redshift for nonevolving galaxies of four spectral types

(E + S0, Sbc, Scd, and Im). The models are derived by convolving filter response functions with spectral energy distributions in Coleman, Wu, & Weedman (1980). These values are then corrected from the AB system to the standard Gunn system (Thuan & Gunn 1976). For each galaxy with redshift, a spectral classification is estimated by comparing the observed $g - r$ color with the model colors at the same redshift. The spectral classification, obtained via interpolation, is treated as a continuous variable between the four spectral types. From the spectral classification, the appropriate K-correction to the r magnitude is then derived using the models.

The r-band absolute magnitudes for the random catalog are generated according to the luminosity function for the data. The luminosity function is modeled as a nonevolving Schechter function (Schechter 1976),

$$\Phi(M_r) = 0.4 \ln 10 \phi^* 10^{0.4(1+\alpha)(M_r^* - M_r)} \exp\left[-10^{0.4(M_r^* - M_r)}\right], \quad (7)$$

where $\Phi(M_r)$ is the comoving number density of objects with absolute magnitude M_r per unit magnitude. The parameters M_r^* and α are determined using the maximum-likelihood method of Sandage, Tammann, & Yahil (1979). For the field sample, $M_r^* \approx -20.5 + 5 \log_{10} h$ and $\alpha \approx -1.2$, consistent with the values found by Lin et al. (1996) for the entire CNOC field sample. To test the assumption that evolution is unimportant over the redshift range of interest, the field sample was split into two further subsamples; the foreground sample, consisting of objects with $z < 0.354$, and the background sample, consisting of objects with $z > 0.390$. The luminosity function was then calculated independently for these two subsamples; no significant difference was detected. The luminosity function is then used as the probability distribution for the absolute magnitudes of the objects in the uniform random catalog. An rest-frame color $(g - r)_0$ is then chosen for each object, so that the distribution of intrinsic colors in the uniform random catalog is the same as that in the data catalog. The r-band absolute magnitude M_r and rest-frame color $(g - r)_0$ for each object are then used to compute the K-corrections, using the method described above.

For each object in the uniform random catalog with apparent magnitude within the sample limits, magnitude and geometric weights w_m and w_{xy} are estimated by interpolating from the data weights. The magnitude weight interpolation is a straightforward one-dimensional interpolation. The two-dimensional geometric weight interpolation is performed by convolving the spatial map of geometric weights of each data object with a Gaussian with a dispersion of 1′. The values of the convolved weights at the position of the random object are then summed, yielding a weight for that random object. The local magnitude weight $w_{\rm lm}$ for the random object is then $w_m \times w_{xy}$; the object is discarded unless $1/w_{\rm lm}$ is less than a randomly chosen number between 0 and 1.

3.2. *The Angular Correlation Function*

The methods described in § 3.1 for generating the random catalog and the weights are tested by comparing the angular correlation functions for the photometric and redshift samples. The angular correlation function w is estimated in a manner similar to that given in equation (6):

$$1 + w(\theta) \approx \frac{R}{D} \frac{\mathrm{DD}(\theta)}{\mathrm{DR}(\theta)}, \quad (8)$$

where the pair counts are now taken over pairs with angular separation θ. If the model (1) for ξ is correct, then

$$w(\theta) = A_w \left(\frac{\theta}{1''}\right)^{-\delta} \quad (9)$$

(Peebles 1980), where $\delta = \gamma - 1$.

The random catalog used for computing w for the redshift sample is generated using the procedure described above, while the catalog for the photometric sample was generated uniformly; both catalogs contain 10,000 objects. Figure 2 shows the results of a power-law fit to the angular correlation for the photometric sample, with δ fixed to 0.7, and w for the redshift sample. The amplitudes in equation (9) are found to be $A_w = 1.4^{+0.3}_{-0.2}$ for the photometric sample and $A_w = 1.3^{+1.2}_{-0.2}$ for the redshift sample; the confidence intervals are the 68% intervals as determined by the bootstrap resampling method discussed in § 3.3 below. The consistency of these amplitudes indicates that the total weights adequately describe the selection effects present in the data. The photometric sample value of A_w implies $w(1') \approx 0.08$, consistent with the value found by Infante & Pritchet (1995) for a sample of objects with $F \leq 22$.

3.3. *Estimating the Uncertainties in the Correlation Function*

All uncertainties given in this paper are calculated using the bootstrap resampling technique. Given a data set with N objects, a large number $N_{\rm bs}$ of resampled data sets are created by randomly selecting N objects from the original

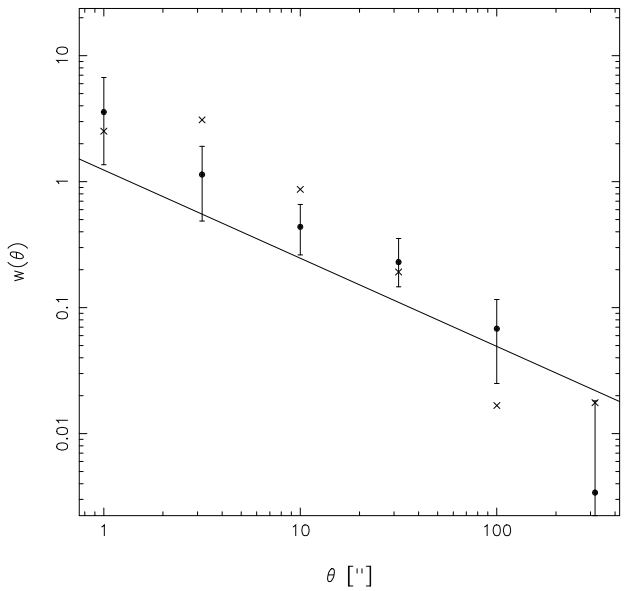

FIG. 2.—Angular correlation function $w(\theta)$ for the photometric and redshift samples. The values of w for the photometric sample are indicated by dots; the data for the redshift sample are indicated by crosses. The error bars are the 68% bootstrap confidence intervals. The solid line is given by the least-squares fit to the photometric data, with δ in eq. (9) fixed to 0.7.

data set (with replacement). The correlation function ξ is then measured for each resampled data set, producing $N_{\rm bs}$ estimates ξ_i ($1 \le i \le N_{\rm bs}$). The uncertainty in the observed correlation function ξ_0 for the original data set is then related to the ξ_i distribution. In earlier work (Ling, Frenk, & Barrow 1986; Fisher et al. 1994a, for example), the uncertainty in the correlation function has been estimated as the standard deviation σ of the resampled correlation function estimates ξ_i; the 1 σ confidence interval is then $\xi = \xi_0 \pm \sigma$. Here, however, we use the bias-corrected 68% confidence interval $\xi \in [\xi_{\rm bc}(0.16), \xi_{\rm bc}(0.84)]$, where

$$\xi_{\rm bc}(t) = G^{-1}(\Phi\{\Phi^{-1}(t) + 2\Phi^{-1}[G(\xi_0)]\}) \tag{10}$$

(Efron & Tibshirani 1986). Here, G is the cumulative distribution function (CDF) of the ξ_i values and Φ is the CDF for the normal distribution. Equation (10) is valid even if the distribution of the ξ_i values is not Gaussian, and even if the median of the ξ_i values differs from ξ_0. The bootstrap method may also be used to estimate the uncertainties in the fit parameters A_w for $w(\theta)$ and r_0 for the projected correlation function $w_p(r_p)$ (discussed in § 3.4); the correlation functions for each resampling are fitted to the appropriate model, yielding $N_{\rm bs}$ values for the fit parameters, A_{wi} or r_{0i}. The resulting CDF is then used, as in equation (10), to estimate the confidence interval for A_w or r_0.

There is evidence (Mo, Jing, & Börner 1992) that the bootstrap method overestimates the uncertainties in the correlation function. This appears to be the case here; the bootstrap uncertainties seem especially large for the projected correlation function $w_p(r_p)$. However, the bootstrap estimator is almost certainly preferable to the Poisson error estimator

$$\sigma_{\xi(r)} \approx \sqrt{\frac{2}{\rm DD(r)}} \tag{11}$$

(Peebles 1973), which is known to be an underestimate of the true uncertainty for correlated data.

3.4. *The Real Space Correlation Function*

Two different correlation functions may be estimated from redshift data; the redshift space correlation function $\xi(s)$ and the real space function $\xi(r)$. If the separation of a pair of objects is computed directly from redshifts, it includes the line-of-sight components of the object's peculiar velocities relative to the Hubble flow. For the range of separations of interest here, the random internal motions of bound groups of objects dominate, elongating structures along the line of sight. This elongation reduces the observed correlation at small separations, so the power-law model (eq. [1]) is expected to be valid only for the real space correlation function.

3.4.1. *Method*

Although it is impossible to measure real space separations directly using only redshift data, it is possible to estimate the parameters of a model for the real space correlation function. This is accomplished by decomposing the redshift space separation of a pair of objects into components parallel and perpendicular to the line of sight to the pair. Since the redshift space distortions act only along the line of sight, functions only of the perpendicular component must be independent of these perturbations.

The decomposition is performed assuming the separations are small, so that the effects of curvature may be neglected. Thus, given two objects with redshifts z_1 and z_2 and angular separation θ_{12}, two vectors $\boldsymbol{x}_i$ ($i = 1, 2$) are formed, such that

$$|\boldsymbol{x}_i| = \frac{2c}{H_0} \frac{\Omega_0 z_i - (2 - \Omega_0)(\sqrt{1 + \Omega_0 z_i} - 1)}{\Omega_0^2 (1 + z_i)}, \quad (i = 1, 2) \tag{12}$$

($\Lambda = 0$), and

$$\boldsymbol{x}_1 \cdot \boldsymbol{x}_2 = |\boldsymbol{x}_1||\boldsymbol{x}_2| \cos \theta_{12} . \tag{13}$$

The comoving redshift space separation of the pair is then $\boldsymbol{s} \approx \boldsymbol{x}_2 - \boldsymbol{x}_1$, and the line of sight to the pair is $\bar{\boldsymbol{x}} = \frac{1}{2}(\boldsymbol{x}_1 + \boldsymbol{x}_2)$. The components of the physical separation parallel and perpendicular to the line of sight are then

$$\pi = \frac{\boldsymbol{s} \cdot \bar{\boldsymbol{x}}}{(1 + \bar{z})|\bar{\boldsymbol{x}}|} \tag{14}$$

and

$$r_p = \sqrt{\left(\frac{|\boldsymbol{s}|}{1 + \bar{z}}\right)^2 - \pi^2} , \tag{15}$$

where $\bar{z} = \frac{1}{2}(z_1 + z_2)$. The definition of the correlation function (eq. [3]) is then generalized to describe the probability in excess of random of finding an object with redshift space separation (r_p, π) from a randomly chosen object. This is estimated as

$$1 + \xi(r_p, \pi) \approx \frac{R}{D} \frac{\rm DD(r_p, \pi)}{\rm DR(r_p, \pi)} , \tag{16}$$

where $\rm DD(r_p, \pi)$ and $\rm DR(r_p, \pi)$ are the weighted number of data-data and data-random ordered pairs with separations (r_p, π), respectively, and D and R are the weighted object counts defined in § 3.1.

Although $\xi(r_p, \pi)$ is affected by the redshift space distortions described earlier, the projected correlation function $w_p(r_p)$, defined by

$$w_p(r_p) = \int_{-\infty}^{\infty} \xi(r_p, \pi) d\pi , \tag{17}$$

is not. Thus,

$$w_p(r_p) = \int_{-\infty}^{\infty} \xi(\sqrt{r_p^2 + x^2}) dx , \tag{18}$$

where the integral is over the real space correlation function. If the power-law model (eq. [1]) is employed, then

$$w_p(r_p) = \sqrt{\pi} \frac{\Gamma(\delta/2)}{\Gamma[(1 + \delta)/2]} r_0 \left(\frac{r_p}{r_0}\right)^{-\delta} \tag{19}$$

(Davis & Peebles 1983). The integral in equation (17) must be truncated at some $\pi_{\rm max}$ for any real data set. The quantity $2\pi \bar{n} J_p(r_p, \pi)$, where

$$J_p(r_p, \pi) = \int_{-\pi}^{\pi} \int_0^{r_p} \xi(r_p', \pi') r_p' \, dr_p' \, d\pi \tag{20}$$

represents the mean number of objects in excess of random within the cylinder with radius r_p and length 2π centered on

an object in the sample; this may be estimated as

$$2\pi\bar{n}J_p(r_p, \pi) \approx \sum_{\substack{r_p' < r_p \\ -\pi < \pi' < \pi}} \left[\mathrm{DD}(r_p', \pi') - \left(\frac{D}{R}\right)\mathrm{DR}(r_p', \pi') \right]. \tag{21}$$

This function is expected to increase with π for small π, approaching some limiting value at large π. Figure 3 shows $2\pi\bar{n}J_p$ (1 h^{-1} Mpc, π) versus π for the extended field sample. As can be seen, cutoffs less than $\sim 3\ h^{-1}$ Mpc exclude real power in $\xi(r_p, \pi)$, while noise appears to be the primary contributor to the integral equation (20) for $\pi \gtrsim 50\ h^{-1}$ Mpc. We adopt 15 h^{-1} Mpc as the cutoff to be used in equation (17); no significant change in the derived correlation length is observed when the cutoff is varied between 5 and 35 h^{-1} Mpc.

3.4.2. *Results*

The projected correlation function $w_p(r_p)$ is calculated for the extended field sample using equations (16) and (17), with the integral truncated at 15 h^{-1} Mpc. The random catalog is generated using the method described in § 3.1; the catalog contains 200,000 objects with redshifts.

The results are shown in Figure 4; r_0 is determined for $\Omega_0 = 1$ and 0.2 by fitting the model equation (19) to the data with δ fixed to 0.7. The correlation length for the extended field sample is found to be $r_0 = 1.9^{+0.4}_{-0.4}\ h^{-1}$ Mpc ($\Omega_0 = 1$) or $r_0 = 2.2^{+0.5}_{-0.4}\ h^{-1}$ Mpc ($\Omega_0 = 0.2$), considerably smaller than the values found locally. As noted in § 3.1, the error bars seem particularly large for $w_p(r_p)$; the least-squares fits give $\chi^2 = 0.13$ ($\Omega_0 = 1$) and $\chi^2 = 0.16$ ($\Omega_0 = 0.2$), indicating that the bootstrap method probably overestimates the uncertainties for this quantity.

As a test of the weighting procedure used to create the extended field sample from the redshift sample, $w_p(r_p)$ was also calculated for the field sample. For the field sample, $r_0 = 1.8^{+0.6}_{-0.3}\ h^{-1}$ Mpc ($\Omega_0 = 1$), or $r_0 = 2.1^{+0.7}_{-0.4}\ h^{-1}$ Mpc ($\Omega_0 = 0.2$). The consistency of the correlation lengths for the field and extended field samples indicates that the weighting

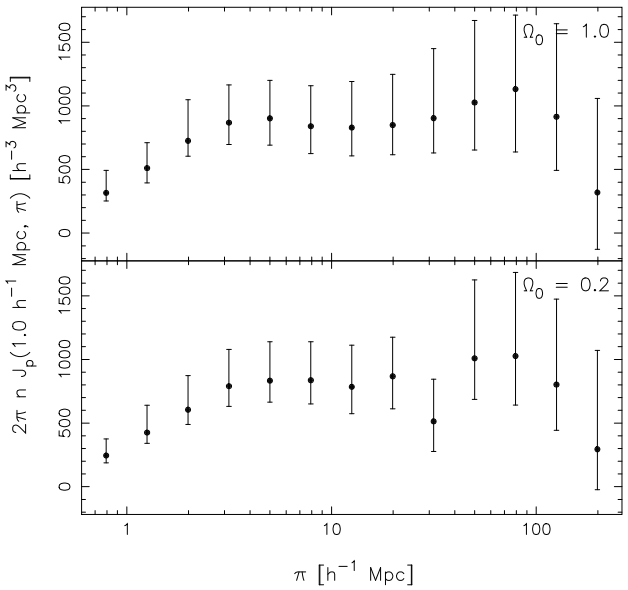

FIG. 3.—Counts in excess of random within a cylinder of radius 1 h^{-1} Mpc and length 2π, $2\pi\bar{n}J_p(1\ h^{-1}$ Mpc, $\pi)$, for the extended field sample, for $\Omega_0 = 1$ and 0.2. The error bars are the 68% bootstrap confidence intervals.

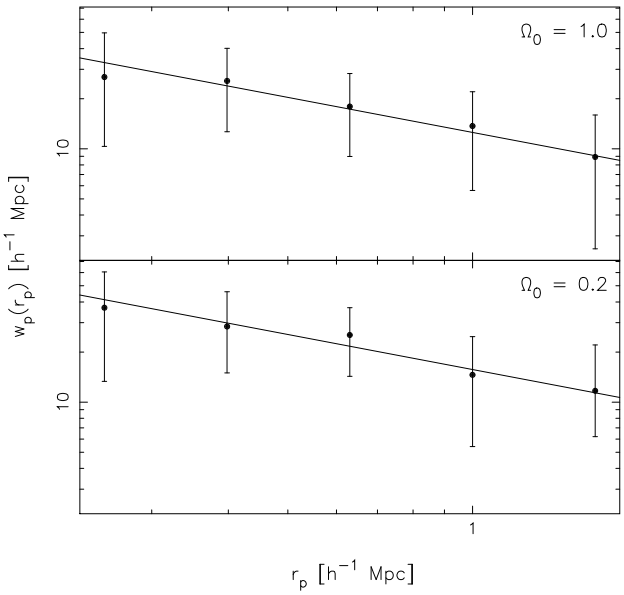

FIG. 4.—Projected correlation function $w_p(r_p)$ for the extended field sample, for $\Omega_0 = 1$ and 0.2. The error bars are the 68% bootstrap confidence intervals. The solid line in each panel is from the least-squares fit of eq. (19) to the data with δ fixed to 0.7.

procedure used for including the cluster galaxies in the extended field sample produces a reasonable estimate of the average value of r_0. The presence of the cluster in the redshift sample causes the correlation length for that sample to be much larger than that for either the field or extended field samples; for the redshift sample, $r_0 = 4.0^{+0.7}_{-0.6}\ h^{-1}$ Mpc ($\Omega_0 = 1$), or $r_0 = 4.2^{+0.7}_{-0.6}\ h^{-1}$ Mpc ($\Omega_0 = 0.2$).

If it is assumed that the population in our sample at $z \sim 0.37$ will evolve to the population observed at $z = 0$ in optical surveys, equation (2) may be used, with $r_0(z = 0)$ equal to the value observed in the local sample, to estimate ε. Applying equation (2), with $r_0 = 1.9\ h^{-1}$ Mpc at $z = 0.37$ and $r_0 = 5.1\ h^{-1}$ Mpc at $z = 0$ yields $\varepsilon \approx 2.2$ ($\Omega_0 = 1$); using $r_0 = 2.2\ h^{-1}$ Mpc at $z = 0$ gives $\varepsilon \approx 1.5$ ($\Omega_0 = 0.2$). Thus, the correlation is found to be evolving rapidly in physical coordinates.

An alternate explanation for the evolution observed in the correlation function is that some of the objects in our sample are weakly clustered and become intrinsically faint at the present epoch (Efstathiou et al. 1991). If the faint population is completely unclustered ($\xi = 0$), and the correlation function of the presently bright objects does not evolve in physical coordinates, then equations (2) and (3) imply that the correlation functions observed at $z = 0$ and at a higher redshift are related by

$$\xi(r, z) = f(z)^2\xi(r, 0)(1 + z)^{-3}, \tag{22}$$

where $f(z)$ is the fraction of objects visible at redshift z which are also visible at $z = 0$. For this extreme limiting case of $\xi = 0$ for the now faint population, our data require that $f \sim 0.8$. While a realistically clustered faint population would require that f be lower, we cannot rule out evolution in the galaxy population as the source of the reduction in r_0 at intermediate redshifts.

3.5. *The Redshift Space Correlation Function*

As noted in § 3.4, the redshift space correlation function is not expected to be a power law because of random peculiar

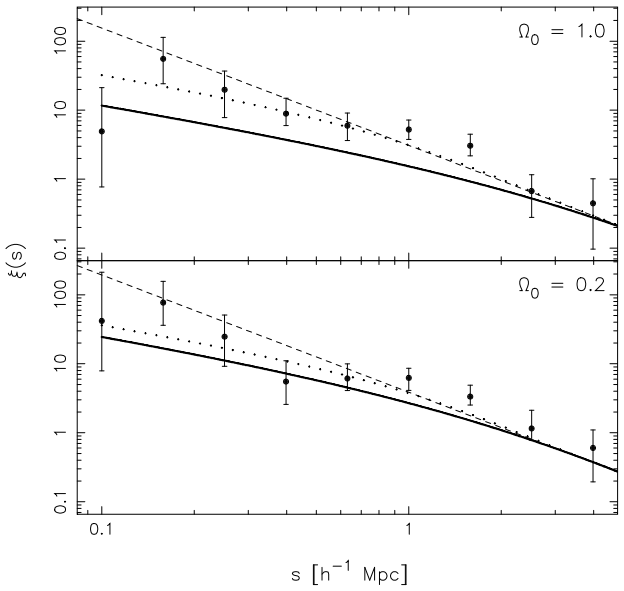

FIG. 5.—Redshift space correlation function $\xi(s)$ for the extended field sample, for $\Omega_0 = 1$ and 0.2. The error bars are the 68% bootstrap confidence intervals. The dashed line in each panel is the power law in eq. (1) with $\gamma = 1.7$ and r_0 taken from the fit to the corresponding projected correlation function data. The solid curve in each panel is given by eq. (27), with $\sigma = 720$ km s^{-1} ($\Omega_0 = 1$) and 360 km s^{-1} ($\Omega_0 = 0.2$). The dotted curve is obtained using a Gaussian with $\sigma = 140$ km s^{-1} in place of the exponential in the velocity distribution model eq. (28).

velocities. However, measurements of $\xi(s)$ can be used, in conjunction with a model for the real space correlation function, to provide information about the velocity distribution of objects in the sample. This, in turn, yields information on the mean matter density.

3.5.1. *Method*

The real space correlation function $\xi(r)$ is related to $\xi(r_p, \pi)$ by

$$1 + \xi(r_p, \pi) = \int g(r, \boldsymbol{v})[1 + \xi(r)]d^3v \tag{23}$$

(Peebles 1980), where $g(r, \boldsymbol{v})$ is the distribution of relative peculiar pairwise velocities of pairs with separation r, and $r^2 = r_p^2 + [\pi - v_z/H(z)]^2$, where v_z is the component of $\boldsymbol{v}$ along the line of sight. To obtain a relation between the redshift space correlation function $\xi(s)$ and the real space correlation function $\xi(r)$, equation (23) is integrated over a sphere of radius s;

$$4\pi\int_{-s}^{s}\xi(s')s'^2ds' = 2\pi\int\int_{-s}^{s}\int_{0}^{(s^2-\pi^2)^{1/2}}\xi(r)g(r, \boldsymbol{v})r_r\,dr_p\,d\pi d^3v\ , \tag{24}$$

using the identity $2\pi\int_{-s}^{s}\int_{0}^{(s^2-\pi^2)^{1/2}}\xi(r_p, \pi)r_p\,dr_p\,d\pi = 4\pi\int_0^s\xi(s')s'^2ds'$.

We employ here a simplified model for the pairwise peculiar velocity distribution in which g is independent of the separation r. Two dimensions of the velocity integral in equation (24) may therefore be performed immediately; we define the line-of-sight peculiar pairwise velocity distribution $f(v_z) = \int_{-\infty}^{\infty}\int_{-\infty}^{\infty} g(v_x, v_y, v_z)dv_x\,dv_y$. Equation (24) then reduces to

$$4\pi\int_0^s\xi(s')s'^2ds' = 2\pi\int_{-\infty}^{\infty}\int_{-s}^{s}\int^{(s^2-\pi^2)^{1/2}}\xi(r)f(v_z)r_p\,dr_p\,d\pi\,dv_z\ , \tag{25}$$

where the integral on the left is over the redshift space correlation function, while the integral on the right is over the real space correlation function. Differentiating equation (25) with respect to s gives the general relationship between the redshift space and real space correlation functions, under the assumption that g is independent of r,

$$\xi(s) = \tfrac{1}{2}s^{-1}\int_{-\infty}^{\infty}\int_{-s}^{s}\xi(\sqrt{s^2 - 2[v_z/H(z)]\pi + [v_z/H(z)]^2}) \times f(v_z)d\pi\,dv_z\ . \tag{26}$$

The argument to the real space correlation function in equation (26) is just the physical separation r, evaluated with $r_p = (s^2 - \pi^2)^{1/2}$. If $\xi(r)$ is modeled as a power law equation (1), then the integral over π in equation (26) may be performed analytically, finally yielding

$$\xi(s) = \frac{1}{2(2-\gamma)}H(z)r_0^{\gamma}s^{-1} \times\int_{-\infty}^{\infty}\left[\left|s + \frac{v_z}{H(z)}\right|^{2-\gamma} - \left|s - \frac{v_z}{H(z)}\right|^{2-\gamma}\right]f(v_z)\frac{dv_z}{v_z}\ . \tag{27}$$

The simplified model for the velocity distribution used here takes f to be an exponential with zero mean and dispersion independent of separation,

$$f(v_z) = \sqrt{\frac{1}{2\sigma^2}}\exp\left(-\sqrt{2}\left|\frac{v_z}{\sigma}\right|\right) \tag{28}$$

(Davis & Peebles 1983). Here, σ^2 is the projected pairwise peculiar velocity dispersion; the three-dimensional mean-square pairwise peculiar velocity $\langle v^2\rangle = 3\sigma^2$ since the mean pairwise peculiar velocity is taken to be zero.

Given a value for the cosmological density parameter Ω_0, σ may be estimated using the cosmic virial theorem,

$$\sigma^2(r, z) = \frac{3H(z)^2\Omega(z)QJr_0(z)^{\gamma}r^{2-\gamma}}{4b(\gamma-1)(2-\gamma)(4-\gamma)} \tag{29}$$

(Peebles 1980; Fisher et al. 1994b), where Q relates the two- and three-point correlation functions, b is the linear bias factor, and J depends only on γ [$J(\gamma = 1.7) = 4.14$]. For γ close to 2, σ is almost independent of separation, consistent with equation (28). Equation (29) depends on the relation between the distributions of galaxies and matter through the (unknown) bias factor, and thus is of limited use as a probe of the true value of Ω_0. Note that according to this model, σ evolves as $(1 + z)^{-\varepsilon/2}$ (holding γ and Q constant).

3.5.2. *Results*

The redshift space correlation function is calculated for the extended field sample using the redshift space analog of

equation (6)

$$1 + \xi(s) \approx \frac{R}{D} \frac{\mathrm{DD}(s)}{\mathrm{DR}(s)}, \quad (30)$$

where DD(s) and DR(s) are the number of data-data and data-random pairs with redshift space separations between s and $s + \Delta s$, respectively. The random catalog used here is the same as that used for computing the real space correlation function. Figure 5 shows $\xi(s)$ for the extended field sample, along with the predictions from equation (27), using $r_0 = 1.9\ h^{-1}$ Mpc, $\gamma = 1.7$, and $\sigma = 720$ km s^{-1} for $\Omega_0 = 1$ and $r_0 = 2.2\ h^{-1}$ Mpc, $\gamma = 1.7$, and $\sigma = 360$ km s^{-1} for $\Omega_0 = 0.2$. These values of σ are computed using equation (29) with $Q = b = 1$. Also shown are the curves given by equation (27) using a Gaussian pairwise peculiar velocity distribution with $\sigma = 140$ km s^{-1}; this value corresponds to the mean velocity uncertainty in the sample of $\sim$100 km s^{-1}.

As can be seen, the $\sigma = 720$ km s^{-1}, $\Omega_0 = 1$ model overestimates the redshift space perturbations. A least-squares fit of equation (27) to the data, using equations (28) and (29), with $\Omega_0 = 1$, $b = 1$, and $\gamma = 1.7$ yields $r_0 = 2.9^{+0.6}_{-0.4}\ h^{-1}$ Mpc, only marginally consistent with the value derived from the projected correlation function data, $r_0 = 1.9^{+0.4}_{-0.4}\ h^{-1}$ Mpc. The $\sigma = 360$ km s^{-1}, $\Omega_0 = 0.2$ model matches the observed $\xi(s)$ more closely, consistent with the low Ω_0 favored by Davis & Peebles (1983) and Fisher et al. (1994b). However, the observed $\xi(s)$ is consistent with a model with zero pairwise peculiar velocity dispersion and redshift space distortions due solely to velocity measurement errors; more data are therefore needed for a precise determination of σ. We conclude that the data are best modeled by a low-density parameter; taking $\Omega_0 = 0.2$, $r_0 = 2.2^{+0.5}_{-0.4}\ h^{-1}$ Mpc and $\sigma = 360$ km s^{-1} yields models which are consistent with both the observed $w_p(r_p)$ and $\xi(s)$.

4. CONCLUSIONS

We have found that the physical correlation length for $0.21 \leq z \leq 0.53$ is $r_0 = 1.9^{+0.4}_{-0.4}\ h^{-1}$ Mpc if $\Omega_0 = 1$, implying $\varepsilon \approx 2.2$ if $r_0 = 5.1\ h^{-1}$ Mpc locally. If $\Omega_0 = 0.2$, $r_0 = 2.2^{+0.5}_{-0.4}\ h^{-1}$ Mpc and $\varepsilon \approx 1.5$. The uncertainties are estimated using the bias-corrected bootstrap resampling method, with 300 resamplings. These results are consistent with earlier results obtained from angular surveys, which indicate rapid evolution (Efstathiou et al. 1991; Infante & Pritchet 1995). It is also consistent with the results from the CFRS (Le Fèvre et al. 1996). This decrease in r_0 from its present value may be interpreted either as a real change in the clustering of the observed galaxies or as caused by a weakly clustered population which composes a substantial fraction of the objects seen at $z \sim 0.37$, but which is intrinsically faint at the present epoch.

The projected pairwise peculiar velocity dispersion at $z = 0.37$, $\sigma = 720$ km s^{-1}, predicted by the cosmic virial theorem using $\Omega_0 = 1$ is somewhat inconsistent with the observed redshift space correlation function; $\Omega_0 = 1$ is therefore weakly rejected. The $\Omega_0 = 0.2$ prediction, $\sigma = 360$ km s^{-1}, however, matches the data more closely. Thus, the relatively small redshift space distortions present favor low Ω_0 as determined from the cosmic virial theorem, consistent with the results of Davis & Peebles (1983) and Fisher et al. (1994b).

More data are required to obtain a precise value for σ and more reliable error estimates. A larger sample would also enable computations of the correlation function for subsamples based on galaxy color or intrinsic brightness, which would help distinguish between the two possible sources of observed evolution described in § 3.4. The CNOC2 redshift survey, presently in progress, will yield $\sim$5000 high-accuracy redshifts in the range $0.15 \leq z \leq 0.7$. This survey will contain enough objects, and sample sufficiently large scales, to permit accurate computations of the redshift space and real space correlation functions and their evolution at intermediate redshifts.

We thank all participants of the CNOC cluster survey for assistance in obtaining and reducing these data. The Canadian Time Assignment Committee for the CFHT generously allocated substantial grants of observing time, and the CFHT organization provided the technical support which made these observations feasible. We gratefully acknowledge financial support from NSERC and NRC of Canada.

REFERENCES

Abraham, R. G., Yee, H. K. C., Ellingson, E., Gravel, P., Carlberg, R. G., Smecker-Hane, T. A., & Pritchet, C. J. 1997, in preparation
Carlberg, R. G. 1991, ApJ, 367, 385
Carlberg, R. G., Yee, H. K. C, Ellingson, E., Abraham, R., Gravel, P., Morris, S., & Pritchet, C. J. 1996, ApJ, 462, 32
Cole, S., Ellis, R., Broadhurst, T., & Colless, M. 1994, MNRAS, 267, 541
Coleman, G. D., Wu, C., & Weedman, D. W. 1980, ApJS, 43, 393
Colin, P., Carlberg, R. G., & Couchman, H. P. M. 1996, ApJ, submitted
Davis, M., & Peebles, P. J. E. 1983, ApJ, 267, 465
Efron, B., & Tibshirani, R. 1986, Stat. Sci., 1, 1, 54
Efstathiou, G. 1995, in Les Houches Session LX, Cosmology and Large-Scale Structure, ed. R. Schaeffer, J. Silk, M. Spiro, & J. Zinn-Justin (Netherlands: Elsevier Science), 133
Efstathiou, G., Bernstein, G., Katz, N., Tyson, J. A., & Guhathakurta, P. 1991, ApJ, 380, L47
Fisher, K. B., Davis, M., Strauss, M. A., Yahil, A., & Huchra, J. 1994a, MNRAS, 266, 50
———. 1994b, MNRAS, 267, 927
Infante, L., & Pritchet, C. J. 1995, ApJ, 439, 565
Koo, D. C., & Szalay, A. S. 1984, ApJ, 282, 390
Le Fèvre, O., Hudon, D., Lilly, S. J., Crampton, D., Hammer, F., & Tresse, L. 1996, ApJ, 461, 534
Lin, H. 1995, Ph.D. thesis, Harvard Univ.
Lin, H., Yee, H. K. C., Carlberg, R. G., & Ellingson, E. 1996, ApJ, submitted
Ling, E. N., Frenk, C. S., & Barrow, J. D. 1986, MNRAS, 223, 21P
Loveday, J., Maddox, S. J., Efstathiou, G., & Peterson, B. A. 1995, ApJ, 442, 457
Mo, H. J., Jing, Y. P., & Börner, G. 1992, ApJ, 392, 452
Peebles, P. J. E. 1973, ApJ, 185, 413
———. 1980, The Large-Scale Structure of the Universe (Princeton: Princeton Univ. Press)
Sandage, A., Tammann, G. A., & Yahil, A. 1979, ApJ, 232, 352
Schechter, P. 1976, ApJ, 203, 297
Thuan, T. X., & Gunn, J. E. 1976, PASP, 88, 543
Yee, H. K. C., Ellingson, E., & Carlberg, R. G. 1996, ApJS, 102, 269